ELEMENTA
Science of the Anthropocene

Nomura, D, et al. 2023. Meltwater layer dynamics in a central Arctic lead: Effects of lead width, re-freezing, and mixing during late summer. *Elem Sci Anth*, 11: 1. DOI: https://doi.org/10.1525/elementa.2022.00102

RESEARCH ARTICLE

Meltwater layer dynamics in a central Arctic lead: Effects of lead width, re-freezing, and mixing during late summer

Daiki Nomura[1,2,3,*], Yusuke Kawaguchi[4], Alison L. Webb[5,6], Yuhong Li [7], Manuel Dall'osto[8], Katrin Schmidt[9], Elise S. Droste[10,11], Emelia J. Chamberlain[12], Nikolai Kolabutin[13], Egor Shimanchuk[13], Mario Hoppmann[11], Michael R. Gallagher[14,15], Hanno Meyer[16], Moein Mellat[16], Dorothea Bauch[17,18], Carolina Gabarró[19], Madison M. Smith[20,21], Jun Inoue[22], Ellen Damm[11,16], and Bruno Delille[23]

Leads play an important role in the exchange of heat, gases, vapour, and particles between seawater and the atmosphere in ice-covered polar oceans. In summer, these processes can be modified significantly by the formation of a meltwater layer at the surface, yet we know little about the dynamics of meltwater layer formation and persistence. During the drift campaign of the Multidisciplinary drifting Observatory for the Study of Arctic Climate (MOSAiC), we examined how variation in lead width, re-freezing, and mixing events affected the vertical structure of lead waters during late summer in the central Arctic. At the beginning of the 4-week survey period, a meltwater layer occupied the surface 0.8 m of the lead, and temperature and salinity showed strong vertical gradients. Stable oxygen isotopes indicate that the meltwater consisted mainly of sea ice meltwater rather than snow meltwater. During the first half of the survey period (before freezing), the meltwater layer thickness decreased rapidly as lead width increased and stretched the layer horizontally. During the latter half of the survey period (after freezing of the lead surface), stratification weakened and the meltwater layer became thinner before disappearing completely due to surface ice formation and mixing processes. Removal of meltwater during surface ice formation explained about 43% of the reduction in thickness of the meltwater layer. The remaining approximate 57% could be explained by mixing within the water column initiated by disturbance of the lower boundary of the meltwater layer through wind-induced ice floe drift. These results indicate

[1] Field Science Center for Northern Biosphere, Hokkaido University, Hakodate, Japan
[2] Faculty of Fisheries Sciences, Hokkaido University, Hakodate, Japan
[3] Arctic Research Center, Hokkaido University, Sapporo, Japan
[4] Atmosphere and Ocean Research Institute, The University of Tokyo, Kashiwa, Japan
[5] School of Life Sciences, University of Warwick, Coventry, UK
[6] Department of Chemistry, University of York, York, UK
[7] Third Institute of Oceanography, Ministry of Natural Resources, Xiamen, China
[8] Institute of Marine Sciences/CSIC, Barcelona, Spain
[9] School of Geography, Earth and Environmental Sciences, University of Plymouth, Plymouth, UK
[10] School of Environmental Sciences, University of East Anglia, Norwich, UK
[11] Alfred Wegener Institute Helmholtz Centre for Polar and Marine Research, Bremerhaven, Germany
[12] Scripps Institution of Oceanography, University of California San Diego, La Jolla, CA, USA
[13] Arctic and Antarctic Research Institute, Saint Petersburg, Russia
[14] Cooperative Institute for Research in Environmental Sciences, University of Colorado, Boulder, CO, USA
[15] National Oceanic and Atmospheric Administration, Physical Sciences Laboratory, Boulder, CO, USA
[16] Alfred Wegener Institute Helmholtz Centre for Polar and Marine Research, Potsdam, Germany
[17] GEOMAR Helmholtz Centre for Ocean Research Kiel, Kiel, Germany
[18] Leibniz Laboratory, University of Kiel (CAU), Kiel, Germany
[19] Barcelona Expert Center (BEC), Institute of Marine Science (ICM-CSIC), Barcelona, Spain
[20] Polar Science Center, Applied Physics Laboratory, University of Washington, Seattle, WA, USA
[21] Woods Hole Oceanographic Institution, Woods Hole, MA, USA
[22] National Institute of Polar Research, Tachikawa, Japan
[23] Unité d'Océanographie Chimique, Freshwater and Oceanic Science Unit of Research (FOCUS), Université de Liège, Liège, Belgium

* Corresponding author:
Email: daiki.nomura@fish.hokudai.ac.jp

that rapid, dynamic changes to lead water structure can have potentially significant effects on the exchange of physical and biogeochemical components throughout the atmosphere–lead–underlying seawater system.

Keywords: Lead, Sea ice, Meltwater, Re-freezing, Mixing, Arctic Ocean

1. Introduction

Sea ice in the Arctic Ocean has decreased in extent, and multi-year ice is being replaced by first-year ice (e.g., Stroeve et al., 2012; Meier et al., 2014; Lindsay and Schweiger, 2015; Kwok, 2018). Changes in sea ice conditions due to thinner, less extensive, and younger sea ice in the Arctic Ocean have had pronounced effects on ice dynamics (e.g., ice deformation and ice drifting speed; Rampal et al., 2011; Spreen et al., 2011). Crack formation and the development of leads in sea ice are strongly related aspects of ice dynamics (Rampal et al., 2011; Spreen et al., 2011; Itkin et al., 2017).

Sea ice lead formation affects the physical, chemical, and biological processes that take place at the interface between the ocean and atmosphere by allowing direct exchange between the two, unrestricted by sea ice (Maykut, 1978; Zemmelink et al., 2005; Petrich et al., 2007; Steiner et al., 2013; Loose et al., 2014; Assmy et al., 2017; Fransson et al., 2017; Nomura et al., 2018; Ólason et al., 2021; Silyakova et al., 2022). Lead width can vary from a few meters to many kilometers (e.g., Wilchinsky et al., 2015). In wintertime, heat and moisture are supplied from the warm surface waters of a lead into the cold atmosphere, and new ice forms at the lead surface (Morison et al., 1992; Morison and McPhee, 1998). In addition, gases such as carbon dioxide and methane are actively exchanged between the lead surface and the atmosphere (Steiner et al., 2003; Fransson et al., 2017; Silyakova et al., 2022). In summertime, meltwater is supplied to the ocean (Eicken, 1994; Richter-Menge et al., 2001; Eicken et al., 2002; Smith et al., 2022), where it occupies the surface of leads during the melt season (Nansen, 1902; Perovich and Maykut, 1990; Richter-Menge et al., 2001; Zemmelink et al., 2005; Golovin and Ivanov, 2015; Nomura et al., 2018), and this less dense low-salinity water is kept at the surface. Meltwater in a lead is also derived from snow meltwater on sea ice that flows into the lead from the sea ice surface and bottom of sea ice (Golovin and Ivanov, 2015; Nomura et al., 2018; Smith et al., 2022). Therefore, during the melting season, leads accumulate meltwater supplied from both above and below the sea ice.

The presence of meltwater creates a strongly stratified environment within leads (Richter-Menge et al., 2001; Golovin and Ivanov, 2015; Nomura et al., 2018) and can form a persistent layer at the surface that may prevent the exchange of heat and gas between seawater and the atmosphere. For a while after formation, leads can act as "windows" for the exchange of heat, gases, vapour and particles (aerosols) to the atmosphere (e.g., Willis et al., 2018; Baccarini et al., 2020; Beck et al., 2021). However, during the melting season, this meltwater layer may reduce atmospheric exchange, because strong stratification restricts water exchange and the shallow meltwater layer equilibrates with the atmosphere, resulting in a small gradient for heat and gas flux between the lead surface and atmosphere. Despite this potential reduction in atmospheric exchange, high concentrations of dimethyl sulfide in the top surface of the meltwater layer (within 0.25 m) under these stratified conditions were observed in Weddell Sea leads (Zemmelink et al., 2005). This observation suggests that stable conditions within a lead and sunlight on the open lead surface enhance biological productivity (Nomura et al., 2018).

Such shallow stratification may weaken as a result of, e.g., tidal mixing (Nomura et al., 2008), wind mixing (Inoue and Kikuchi, 2006), or ice movement during a high wind event (Richter-Menge et al., 2001). Golovin and Ivanov (2015) showed that lead water dynamics changed across seasonal transitions. As the water at the surface of a lead cools, the water density in the lead increases. In addition, as the surface water freezes, brine is rejected, and this process promotes vertical mixing (Morison and McPhee, 1998).

Understanding processes that contribute to the collapse of stratification in the lead, which are intricately related and difficult to examine separately, requires detailed observations. However, field surveys of leads are challenging, especially in autumn, when the ice extent and thickness are at their minimum and the leads are beginning to freeze. During a typical voyage, observations are carried out at one station for several days, and then the ship moves on. As a result, there are few long-term observations of phenomena such as open water (Richter-Menge et al., 2001) or refrozen leads (Kauko et al., 2017). In addition, surveys during late autumn in an environment where the amount of sea ice has decreased in recent years can be carried out only in the central Arctic.

During the Multidisciplinary drifting Observatory for the Study of Arctic Climate (MOSAiC) expedition, year-round observations were conducted in the central Arctic Ocean from 2019 to 2020 (e.g., Nicolaus et al., 2022; Rabe et al., 2022; Shupe et al., 2022). We had the opportunity to carry out intensive fixed-point observations of the physical components of lead water over a 4-week survey, from the end of the melting period to the beginning of the freezing period. In this study, we investigated in detail the water structure in a lead. We conducted fixed-point observations to investigate the physio-chemical dynamics of the meltwater layer in the lead, and used stable oxygen isotopes to infer the origin of the meltwater. By observing changes in the meltwater layer caused by the opening and closing of the lead, we evaluated the effect of external factors on the thickness of the meltwater layer. We also investigated changes in the water structure within the lead as freezing progressed and evaluated the meltwater balance between

the lead water and the under-ice water. Finally, we examined the vertical mixing by disturbance of the lower boundary of the meltwater layer by wind-induced ice floe drift. The results of these surveys contribute to an understanding of changes in the composition of gases in leads, gas exchange with the atmosphere, and the biogeochemistry of lead water (Parmentier et al., 2013), which will be addressed in future studies.

2. Materials and methods

2.1. Lead formation

Sea ice lead surveys were carried out during MOSAiC Leg 5 (August 21 to September 20, 2020) in the multi-year pack ice region of the central Arctic Ocean (**Figure 1**). During Leg 4, R/V *Polarstern* drifted to the ice edge in the Fram Strait. Thereafter, R/V *Polarstern* was relocated to the Central Arctic to study the onset and early freezing phase of the sea ice. On August 22, a crack about 0.5 m wide and 300 m long formed off the stern of R/V *Polarstern* and extended in the starboard direction (**Figure 1**). Water sampling was undertaken from the sea ice alongside the lead (Stations 3 and 8; **Figure 1**; **Table 1**). On August 24, the crack expanded, forming a lead with a width of approximately 50 m. During the 4-week survey period, the lead width varied dramatically (see Section 3.4 for details) and was monitored during the survey period by visual observations from Stations 3 and 8 for each observation day. Aerial photographs were taken by a drone with scale on August 25 and 29, which were used to calibrate subsequent visual determinations of lead width.

2.2. Hydrographic observations and water sampling within the lead

Vertical profiles of temperature and salinity in the lead water were obtained with a RINKO Profiler (model ASTD103, JFE Advantech, Japan) at Stations 3 and 8 on a daily basis for the initial 2 weeks of the survey, and on a weekly basis during the second half of the survey period (**Figure 1**; **Table 1**; Nomura et al., 2022). The accuracy of temperature and salinity is ± 0.01°C and ± 0.01, respectively. When the surface was frozen, a 0.15 m $\times$ 0.15 m hole was cut with a hand saw 0.5 m away from the thick ice (1.6 m) at the edge of the lead, and ice thickness was measured before a RINKO profiler was lowered into the lead water. The RINKO profiler was lowered on a rope by hand to a depth of about 5 m very slowly and carefully so as not to disturb the structure of the meltwater layer. The down-cast data were used because the structure of the meltwater layer was disturbed when the RINKO Profiler was recovered (up-cast).

To obtain discrete water samples from the lead, the vertical structure and depth of the meltwater layer were checked from the same hole used for the RINKO Profiler by attaching a conductivity sensor (Cond 315i, WTW GmbH, Germany) to a 2 m length ruler and inserting the ruler into the lead water until the salinity measured by Cond 315i increased at the meltwater–seawater interface (**Table 1**). Water was pumped up with a peristaltic pump (Masterflex E/S Portable Sampler, Masterflex, USA) through a 2 m long PTFE tube (L/S Pump Tubing, Masterflex, USA) at depths of 0.1 m, 0.7 m, and 1.0 m on August 29 (Station 3) and at depths of 0.1 m, 0.3 m, and 1.0 m on September 15 (Station 8). Salinity was measured at each depth by attaching a conductivity sensor (Cond 315i, WTW GmbH, Germany). The tube intake was likewise attached to the bottom of the ruler. Water samples to measure stable oxygen isotopes ($\delta^{18}O$) were collected in 50-mL glass screw-cap narrow-neck vials (VWR international LLC, Germany). Discrete water sampling took place after vertical profiles of temperature and salinity were obtained using the RINKO Profiler (**Table 1**).

2.3. Lead ice and underway water sampling

Ice in the lead was collected at Station 8 on September 15. A 0.25 m $\times$ 0.25 m $\times$ 0.13 m thick ice block was cut with a hand saw and placed into a zip-lock bag. Ice temperature at the surface was measured with a needle-type temperature sensor (Testo 110 NTC, Brandt Instruments, Inc., USA). Ice samples were immediately placed in a cooler box along with ice packs to keep their temperature low and minimize brine drainage. Onboard R/V *Polarstern*, ice samples were transferred into ice melting bags (Smart bags PA, AAK 5 L, GL Sciences Inc., Japan) and melted in the dark at 4°C. After the ice melted, the meltwater was placed in a 30-mL glass screw-cap vial for later $\delta^{18}O$ measurement and into a 100-mL polypropylene bottle (I-Boy, AS ONE Corporation, Japan) for later salinity measurement. These samples were stored at 4°C in the dark until analysis.

Seawater samples (from a depth of about 10 m) were collected via the underway water sampling system of the R/V *Polarstern* during Leg 5 (**Table 1**). Samples were placed into 250-mL glass vials (Duran Co. Ltd, Germany) for later $\delta^{18}O$ and salinity measurements.

2.4. Sample analysis

Salinity (practical salinity scale, dimensionless) of collected samples was determined with the same conductivity sensor used on sea ice (Cond 315i, WTW GmbH, Germany). Oxygen isotope analyses were carried out with a mass spectrometer (DELTA-S Finnigan MAT, USA) at the ISOLAB Facility at AWI Potsdam employing the equilibration method (details in Meyer et al., 2000; Meyer et al., 2022). Values of $\delta^{18}O$ in per mil (‰) were calculated using the $^{18}O/^{16}O$ ratio of Vienna standard mean ocean water (V-SMOW) as the standard. The standard deviation of $\delta^{18}O$, calculated from 6 subsamples of the reference water ($\delta^{18}O = -0.07$‰) was <0.05‰.

2.5. Definition of meltwater layer thickness

In this study, the meltwater layer thickness in each profile was defined by the depth of the actual maximum of the density gradient (>0.1 kg m^{-3} cm^{-1}).

2.6. Fractions of snow and sea ice meltwaters and under-ice seawater in the lead water

To clarify the origin of the meltwater within the lead, the fractions of snow meltwater, sea ice meltwater, and seawater were estimated with the following equations (Østlund and Hut, 1984) for the discrete water samples obtained on August 29 and September 15:

$$F_{\mathrm{snow}} + F_{\mathrm{si}} + F_{\mathrm{sw}} = 1 \quad (1)$$

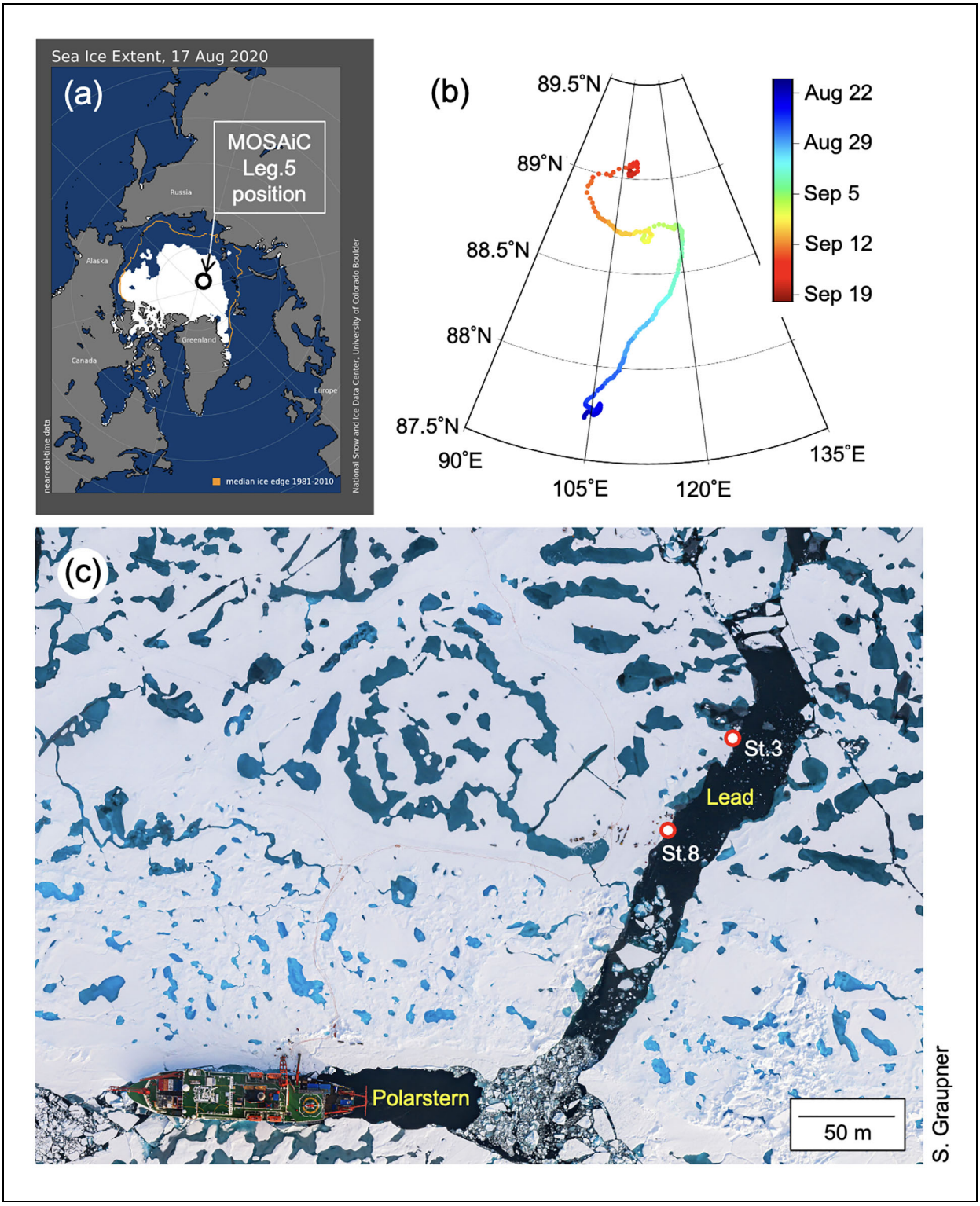

Figure 1. Location of this lead study on the MOSAiC Leg 5 ice floe. (a) Sea ice extent over the Arctic Ocean (National Snow and Ice Data Center, University of Colorado, Boulder) on August 17 and the position of the MOSAiC Leg 5 ice floe. (b) Drift trajectory during MOSAiC Leg 5. (c) Map of the sampling location on the MOSAiC Leg 5 ice floe, showing the *Polarstern*, the lead, and Stations 3 and 8. This image was obtained on August 25, 2020, by a drone (operated by S. Graupner).

$$F_{\mathrm{snow}}\, S_{\mathrm{snow}} + F_{\mathrm{si}}\, S_{\mathrm{si}} + F_{\mathrm{sw}}\, S_{\mathrm{sw}} = S_{\mathrm{obs}} \quad (2)$$

$$F_{\mathrm{snow}}\, \Delta_{\mathrm{snow}} + F_{\mathrm{si}}\, \Delta_{\mathrm{si}} + F_{\mathrm{sw}}\, \Delta_{\mathrm{sw}} = \Delta_{\mathrm{obs}} \quad (3)$$

where F, S, and Δ represent the fraction, salinity, and $\delta^{18}O$, respectively. The subscripts "snow," "si," "sw," and "obs" refer to snow meltwater, sea ice meltwater, seawater, and measured values of the observed water, respectively. The fractions obtained with Equations 1–3 are expressed as percentages. The end-member values for snow, sea ice, and seawater are shown in **Table 2**. For end-member values of snow and sea ice, we used the values obtained during Leg

Table 1. Sampling date, time, station, and activity

Date (in 2020)	Time (UTC)	Station	Activity
Aug 21	12:06	R/V *Polarstern*	Underway water sampling
Aug 22	05:45	R/V *Polarstern*	Underway water sampling
Aug 22	15:54	R/V *Polarstern*	Underway water sampling
Aug 23	11:59	Station 3 1st	Rinko CTD cast
Aug 23	12:04	Station 8	Rinko CTD cast
Aug 23	12:37	Station 3 2nd	Rinko CTD cast
Aug 23	20:12	R/V *Polarstern*	Underway water sampling
Aug 24	13:12	Station 3	Rinko CTD cast
Aug 24	13:37	Station 8	Rinko CTD cast
Aug 24	18:58	R/V *Polarstern*	Underway water sampling
Aug 25	09:45	Station 8	Rinko CTD cast
Aug 25	12:47	Station 3	Rinko CTD cast
Aug 26	17:14	R/V *Polarstern*	Underway water sampling
Aug 27	08:46	Station 3	Rinko CTD cast
Aug 28	10:44	Station 3	Rinko CTD cast
Aug 29	06:13	Station 3	Rinko CTD cast
Aug 29	06:33	Station 3	Water sampling
Aug 30	09:23	Station 3	Rinko CTD cast
Sep 1	09:43	Station 3	Rinko CTD cast
Sep 3	08:20	Station 3	Rinko CTD cast
Sep 4	11:07	Station 3	Rinko CTD cast
Sep 8	08:46	Station 3	Rinko CTD cast
Sep 10	05:36	R/V *Polarstern*	Underway water sampling
Sep 11	19:25	R/V *Polarstern*	Underway water sampling
Sep 12	02:52	R/V *Polarstern*	Underway water sampling
Sep 13	09:00	Station 8	Rinko CTD cast
Sep 15	02:25	R/V *Polarstern*	Underway water sampling
Sep 15	09:10	Station 8	Lead ice sampling
Sep 15	09:19	Station 8	Rinko CTD cast
Sep 15	09:30	Station 8	Water sampling
Sep 17	06:13	Station 8	Rinko CTD cast
Sep 20	13:52	R/V *Polarstern*	Underway water sampling

4 (Lange et al., n.d.) which might have contributed to the observed meltwater layers. Leg 5 samples for snow and sea ice were already affected by melting, suggesting that they were not appropriate to use as end-member values. For the end-member value of seawater, we used the highest salinity seawater measured during Leg 5 (32.6 at 10 m depth on August 22, a salinity that was higher than that of the end-member of seawater for Leg 4). At the end of August, an abrupt freshening occurred when the ice floe moved across a surface frontal structure and entered a new region (see Section 4.4 for details). Therefore, we used high-salinity and low-salinity end-member values for discrete water samples obtained on August 29 and September 15, respectively (**Table 2**). The mean difference of the fraction within the changing of the standard deviations of the salinity and $\delta^{18}O$ measurements for each end-member value was 1.9%.

3. Results

3.1. Temporal variations of air temperature, wind speed, and ice drift speed

Figure 2a shows the temporal variations in air temperature, as reported by Schmithüsen et al. (2021). During the first half of the survey period (end of August), air temperature remained steady around 0°C, whereas in the first days of September (second half of the survey period), air temperature steadily decreased to below −10°C as the system approached the autumn freeze up (Shupe et al., 2022). Wind speeds exceeding 12 m s^{-1} were observed during two storm events: one around September 7 and the other around September 13 and 14 (**Figure 2b**). A sudden air temperature increase was observed around September 13 and 14 during the second storm (**Figure 2a**). The ice drift speed varied between 0 and 36 km d^{-1} with highest drift speeds during the storm events (**Figure 2c**).

3.2. Temporal variations of lead width, meltwater layer thickness, and ice thickness in the lead

Figure 2d shows the temporal variations in lead width. At the start of the survey on August 23, there was a crack 0.5 m wide, which opened to a 50 m wide lead before dawn on August 24. Subsequently, the lead width narrowed gradually through the first half of the survey period down to 5 m, then remained stable after September 1 (**Figure 2d**).

The meltwater layer thickness varied between 0 and 0.8 m (**Figure 2e**). At the beginning of the survey period (August 23), the meltwater layer was 0.8 m thick, but the thickness dropped to 0 m on August 24 (Station 3) before increasing again to 0.6 m on August 28. In the second half of the survey period, the meltwater layer thickness decreased from 0.4 m on September 3 to 0 m on September 17.

At the beginning of the survey period, there was a combination of open water and very thin ice (0.02–0.03 m) at the lead surface (**Figure 2f**). However, after the beginning of September and the onset of freeze up, ice thickness in the lead increased with time, eventually becoming 0.2 m

thick on September 17. In this study, we defined the lead freeze-up date based on the regression line fitted to the data after September 6, where a clear increase of lead ice thickness was confirmed ($r^2 = 0.89$, $p < 0.001$; **Figure 2f**). For this regression line, September 1 was the date when the intercept was zero. Therefore, in this study, "before freezing" refers to the time period until August 31, and "after freezing" refers to the period after that date (September 1 onwards).

Table 2. End-member values (mean ± standard deviation) for snow, sea ice, and seawater

End-Member	Salinity	$\delta^{18}O$ (‰)
Snow[a]	0	−19.1 ± 9.8
Sea ice[a]	2.4 ± 0.3	−0.39 ± 0.47
Seawater[b]	32.6	−1.25
Seawater[c]	29.7	−3.18

[a]From Lange et al. (n.d.). The n value is 67 for snow and 21 for sea ice.

[b]From 10 m depth on August 22.

[c]From 10 m depth on September 15.

3.3. Vertical profiles of salinity, temperature, and density within the lead

Figure 3 shows temporal variations in the vertical profiles of salinity, temperature, and density in the lead obtained with the RINKO Profiler. Salinity in the water column down to 5 m depth ranged from 0.6 (0.01 m depth on August 23 at Station 3) to 31.6 (4.8 m depth on August 23 at Station 3) (**Figure 3a** and **b**). At the beginning of the survey period (August 23), low-salinity (near zero) water occupied the top 0.8 m. The temperature of this water was higher than 0°C, and its density was low (around 1000 kg m^{-3}; **Figure 3c–e**). Most of the time, this low-salinity, low-density, and high-temperature

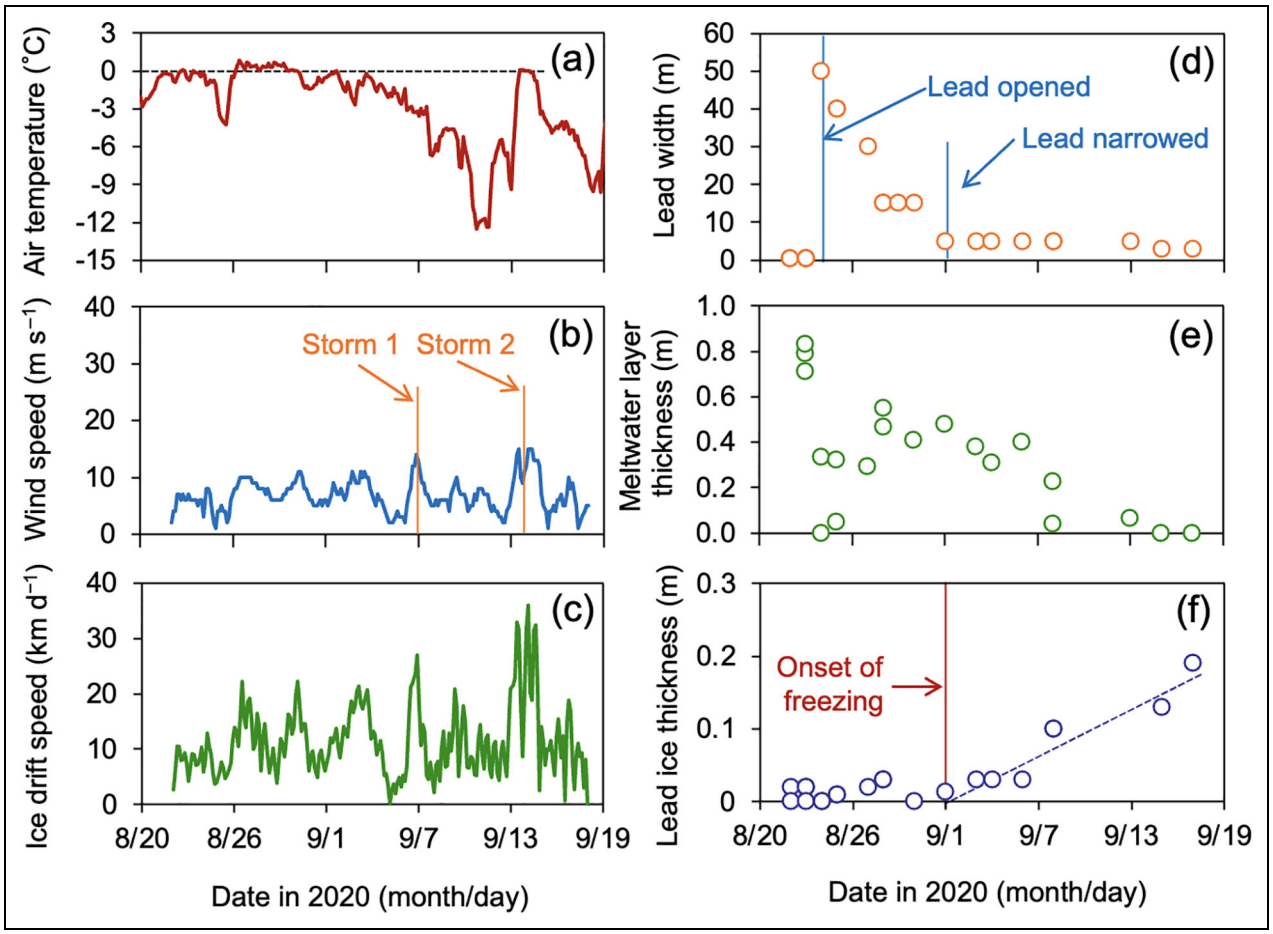

Figure 2. Temporal variation in meteorological and ice conditions. Temporal variations of (a) air temperature; (b) wind speed, with the two storms of the study period indicated; (c) ice drift speed; (d) lead width, with the opening and narrowing dates indicated; (e) meltwater layer thickness, and (f) ice thickness in the lead, with the onset of freezing indicated. Data for air temperature, wind speed, and position to calculate the ice drift speed are from Schmithüsen et al. (2021). For (a) and (b), data were obtained at 3-hour intervals from the mast of R/V *Polarstern* at 25 m height. For (c), drift speed was calculated based on the drift distance every 3 hours based on the position of R/V *Polarstern* (Rex, 2021). The dashed line in (f) is a regression line fitted to the data after September 6 to define the onset date of freezing (September 1).

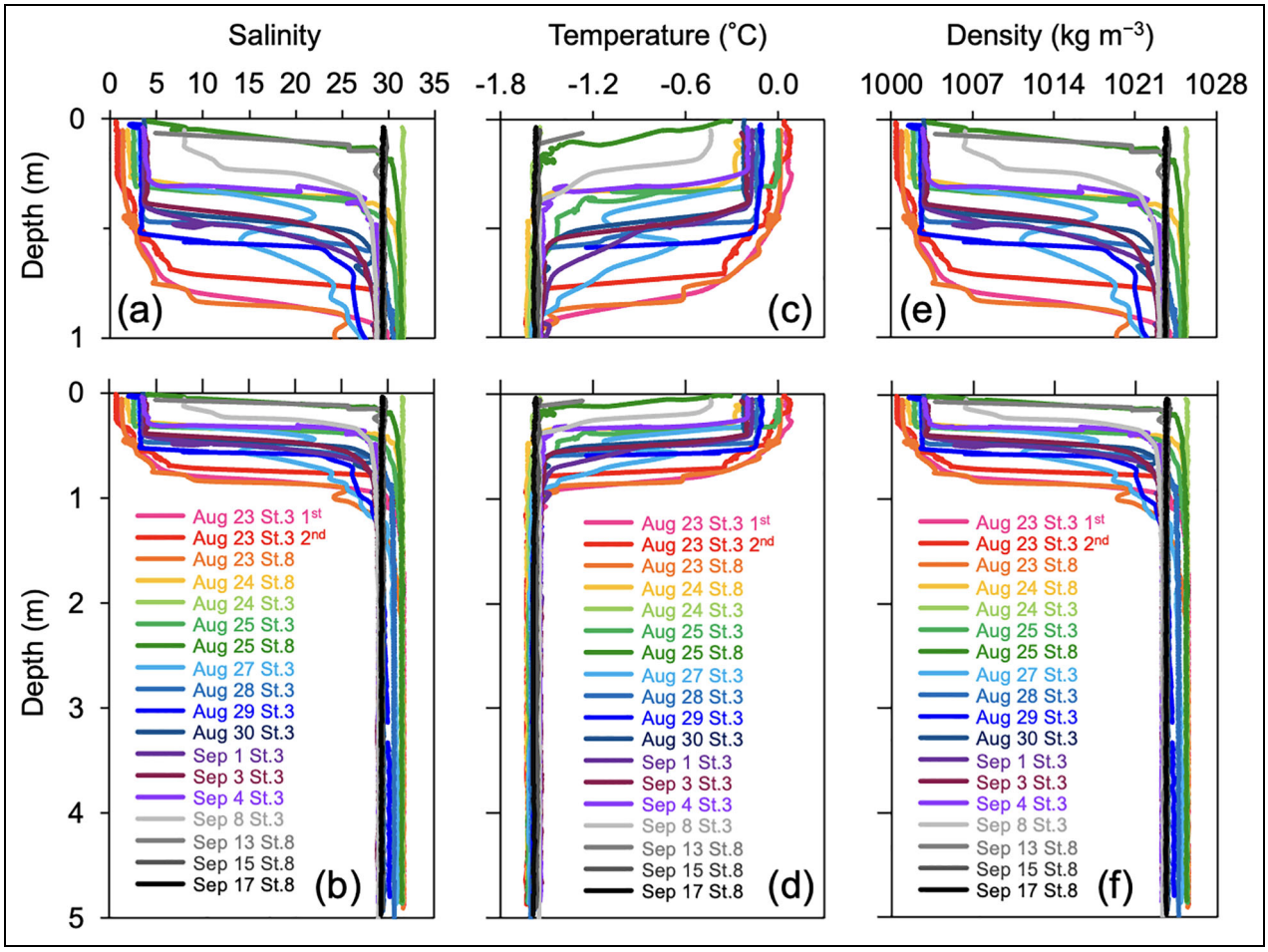

Figure 3. Temporal variations in the vertical profiles of physical oceanographic parameters. Temporal variations in the vertical profiles of (a, b) salinity, (c, d) temperature, and (e, f) density in the lead obtained by the RINKO Profiler. Enlarged views of the upper meter of the vertical profiles for (b), (d), and (f) are shown in (a), (c), and (e), respectively.

water layer was present, but the layer became generally thinner and colder as the survey period progressed. By the end of the period (e.g., September 15 and 17), profiles became vertically uniform (**Figure 3**).

3.4. Vertical profiles of $\delta^{18}O$ and fractions of snow, sea ice meltwater, and under-ice seawater in the lead

Figure 4a shows the depth profiles of $\delta^{18}O$ and salinity based on discrete water sampling. Similarly to the RINKO Profiler data (**Figure 3a** and **b**), salinity at the lead surface (0.1 m) was low (3.2) and increased with depth. At depths of 0.7 m and 1 m in the lead, salinity was about 30.0. In contrast, $\delta^{18}O$ was relatively constant (-2.7 ± 0.2‰) at all depths (**Figure 4a**). The fractions of each component (snow, sea ice meltwater, and seawater) of the lead water changed with depth (**Figure 4b**). At the surface, 83% of the lead water was composed of sea ice meltwater and about 13% was snow meltwater, whereas at depths of 0.7 m and 1.0 m, the lead water consisted mostly of seawater (>91%).

In the lead (Station 8) on September 15, the value of each parameter became vertically uniform: salinity was 29.1–29.2 and $\delta^{18}O$ was -3.2‰ (**Figure 4a**). In addition, the lead water consisted mostly of seawater (>98%; **Figure 4b**).

3.5. Temporal variations of salinity and $\delta^{18}O$ of seawater

Figure 5 shows the temporal variations in the upper water column of salinity at 3 m and 10 m depths (**Figure 5a**) and $\delta^{18}O$ at 10 m depth (**Figure 5b**). The salinity at both 3 m and 10 m decreased by more than 3, from 32.6 on August 22 (10 m depth) to 29.3 on September 17 (3 m depth). The $\delta^{18}O$ at 10 m depth also decreased from -1.25‰ on August 21 to -3.18‰ on September 15.

3.6. Temperature, salinity, and $\delta^{18}O$ of lead ice

Temperature (ice surface), salinity (bulk), and $\delta^{18}O$ for the lead ice (0.2 m thick) collected on September 15 at Station 8 was -2.3°C, 4.3, and -1.25‰, respectively.

4. Discussion

4.1. Characteristics of the meltwater layer in the lead

Numerous studies in both the Arctic and Southern Ocean sea ice regions have observed the presence of a meltwater layer in leads (Nansen, 1902; Perovitch and Maykut, 1990;

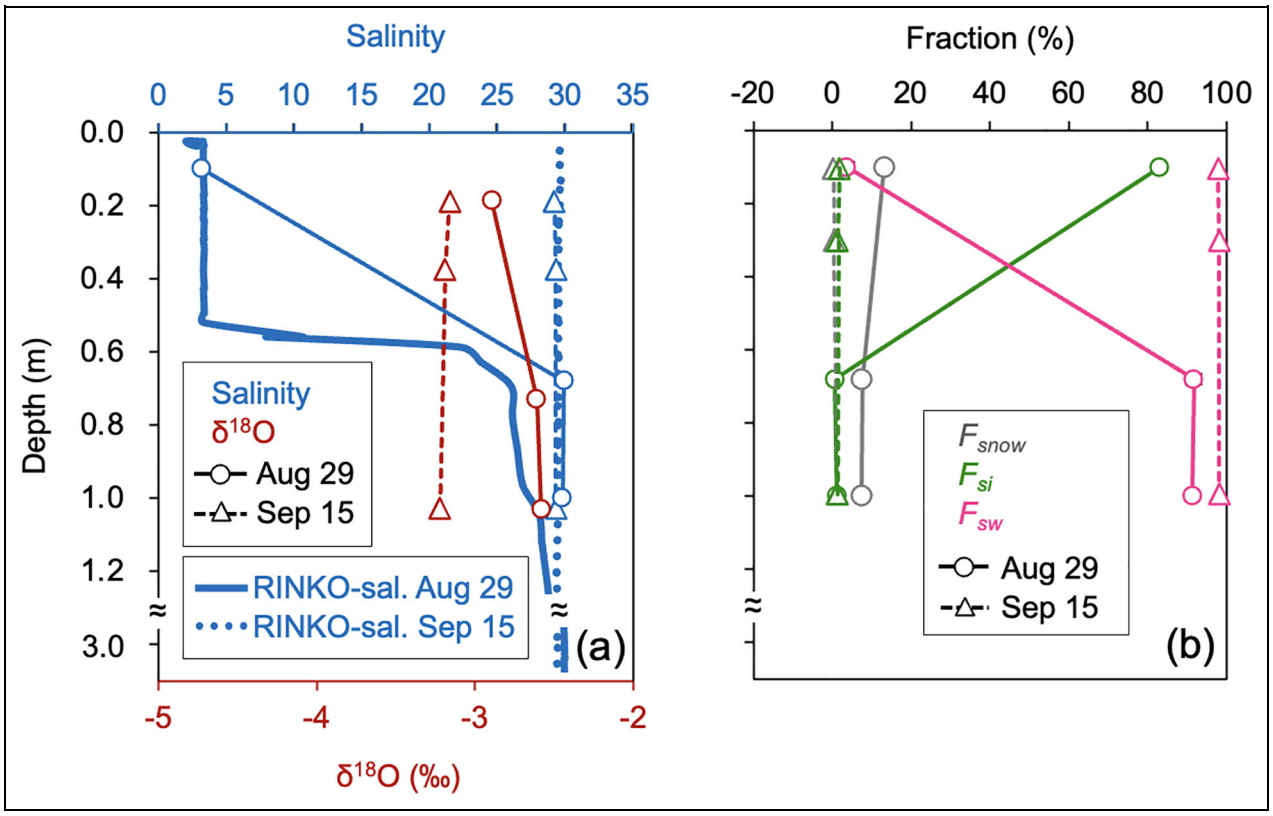

Figure 4. Vertical profiles for salinity, $\delta^{18}O$, and fractions of snow, sea ice, and seawater. (a) Changes in $\delta^{18}O$ (red) and salinity (blue) with depth based on discrete water samples collected at Station 3 on August 29 (circles and thin lines) and Station 8 on September 15 (triangles and dashed lines). Salinity profiles obtained by the RINKO Profiler are indicated for August 29 (thick blue line) and September 15 (dotted blue line). (b) Changes in the fractions of snow (F_{snow}), sea ice meltwater (F_{si}), and seawater (F_{sw}) with depth in the lead for each sampling date.

Richter-Menge et al., 2001; Zemmelink et al., 2005; Golovin and Ivanov, 2015; Nomura et al., 2018), ranging in thickness from a few centimeters to a few meters. For example, Richter-Menge et al. (2001) observed a 1.2 m thick meltwater layer in a lead surrounded by 1.5–2.0 m thick ice in the middle of July 1998 at the drifting ice station (the Seattle site) in the Beaufort Sea during the Surface Heat Budget of the Arctic Ocean (SHEBA) experiment. The salinity in the meltwater layer was 0.7–0.9, and its temperature ranged from 0.9°C to 1.5°C (Richter-Menge et al., 2001). However, the winds soon increased, and the thickness of the meltwater layer decreased to 1.0 m. At the end of July 1998, the meltwater layer was only 0.4 m thick, and by the beginning of August, it had disappeared. The disappearance of the layer coincided with an increase in the ice drift speed around the site, as well as with an increase in their differential motion (Richter-Menge et al., 2001).

Golovin and Ivanov (2015) studied detailed seasonal changes of a meltwater layer with a thickness of about 2 m (maximum) in a lead at the Russian SP-31 drifting ice station in the Beaufort Sea from the end of May to the middle of September 1990. They observed five seasonal stages of lead water dynamics: (1) transition from winter to summer conditions (May 26 to June 17); (2) intensive snow melting and the beginning of sea ice melting (June 17–26); (3) intensive sea ice melting (June 26 to July 22); (4) weak sea ice melting (July 22 to August 16); and (5) steady ice formation in the lead and transition to winter conditions (August 16 to September 18). The changes observed in our study were similar to those of the fourth and fifth stages of their study. The $\delta^{18}O$ meltwater signal indicated the dominance of sea ice meltwater (**Figure 4b**) (third and fourth stages) over snow meltwater in the meltwater layer (second stage). Smith et al. (2022) reported that the under-ice meltwater layer was composed of approximately 58% sea ice meltwater, 11% snow meltwater, and 31% seawater during Leg 4 (at the ice edge in Fram Strait during July 2020). Our results support the assertion that sea ice meltwater was supplied to the lead surface from the bottom of the sea ice.

4.2. Relationship between meltwater layer thickness and lead width

Figure 6a shows the relationship between lead width and meltwater layer thickness. At first glance, there is no apparent relationship. However, when data collected before and after freezing at the beginning of September (e.g., on September 1) were considered separately, a strong negative correlation ($r^2 = 0.77$, $p < 0.001$) was found between lead width and the meltwater layer thickness before freezing (red circles in **Figure 6a**). Therefore, prior to freezing, changes in lead width determined the thickness of the meltwater layer in the lead.

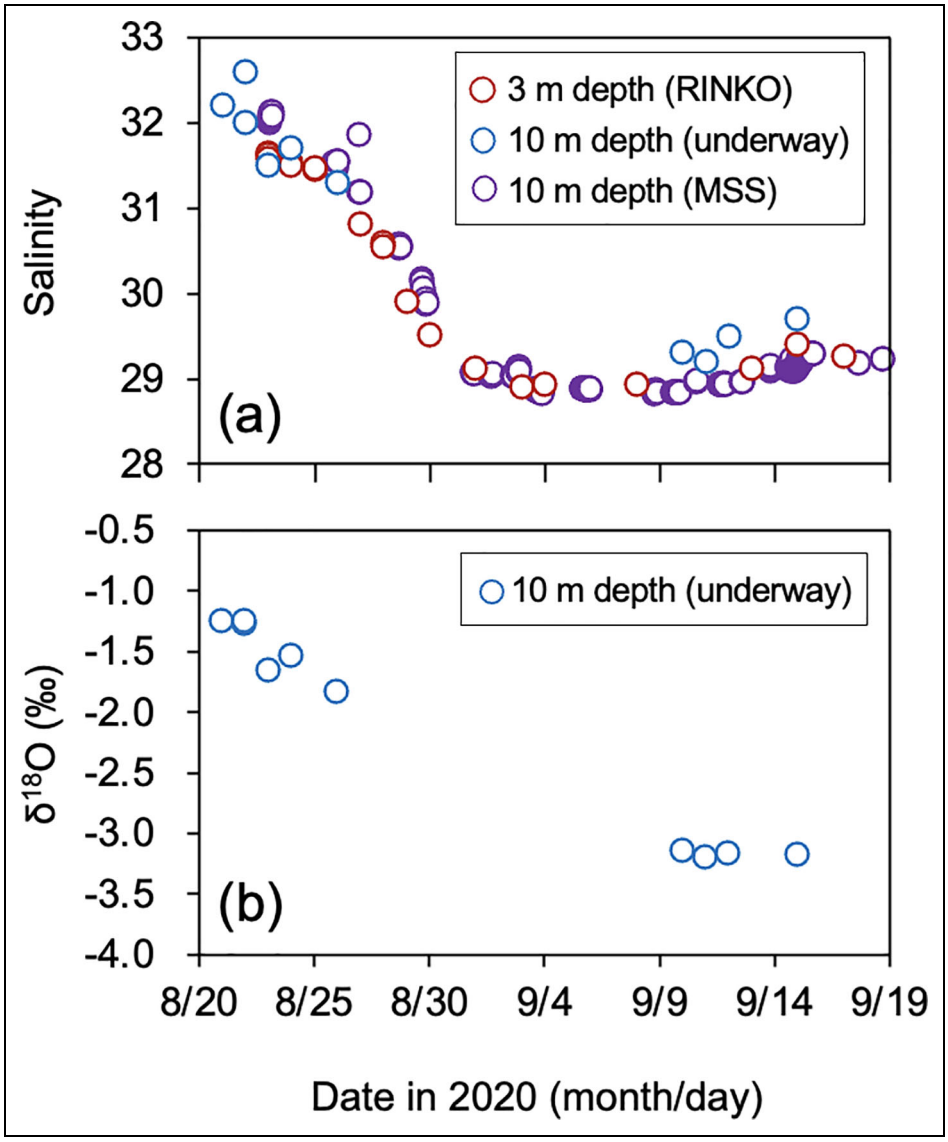

Figure 5. Temporal variations of salinity and $\delta^{18}O$ at depths of 3 m and 10 m. Temporal variations of (a) salinity at 3 m and 10 m depths and (b) $\delta^{18}O$ of the seawater at 10 m depth. Data for 3 m depth was obtained by the RINKO Profiler. Data for 10 m depth was obtained by the underway water sampling system (blue) and MSS profiler (purple; Schulz et al., 2022).

Next, we examined the reason for this relationship, which is illustrated schematically in **Figure 7a** and **b**. When the lead was narrow (e.g., on August 23), the meltwater layer was thick (about 0.7–0.8 m for Station 3 and 0.8 m for Station 8), whereas when the crack expanded rapidly on August 24, forming a 50 m wide lead, the meltwater layer disappeared at Station 3 (**Figure 2d** and **e**). This change is also clear in the vertical salinity profiles: On August 24, the salinity was about 31.6 throughout the water column at Station 3 (**Figure 3a** and **b**). This result suggests that the meltwater layer was stretched by the rapid widening of the lead. For Station 8, although the meltwater layer became thinner (0.3 m) due to stretching on August 24, it did not completely disappear (**Figures 2e**, **3a**, and **6a**), suggesting spatial heterogeneity in lead water structure within the same lead. However, variations between lead width and meltwater layer thickness (meltwater layer became thinner due to stretching by the widening of the lead) were similar for both stations (**Figure 6a**). This similarity matches findings at the SHEBA drifting ice station in the Beaufort Sea, where the disappearance of the meltwater layer coincided with an increase in the ice drift speed and in their differential motion (Richter-Menge et al., 2001). In our study, the meltwater layer disappeared on August 24 (Station 3) right after the rapid expansion of the lead. Interestingly, the thickness of the meltwater layer recovered to 0.6 m on August 29 with the narrowing of the lead (**Figure 2d** and **e**). These findings support the inferred relationship between lead width and meltwater layer thickness depicted in **Figure 7a** and **b**.

We next examined the relationship between changes in lead width and wind speed and ice drift speed (**Figure 2b**–**d**). On August 24, when the crack expanded rapidly to a lead with a width of 50 m (**Figure 2d**), neither the wind speed (**Figure 2b**) nor the ice drift speed (**Figure 2c**)

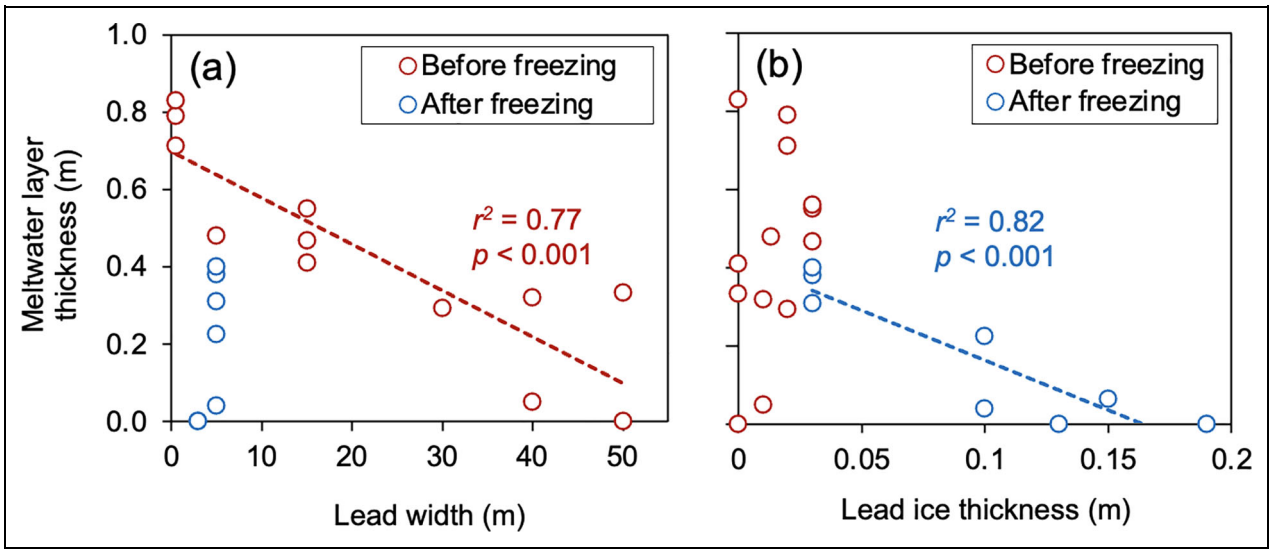

Figure 6. Relationships between meltwater layer thickness and lead width and ice thickness. Scatter diagrams of the relationship between meltwater layer thickness and (a) lead width and (b) lead ice thickness. The red dashed line in (a) is a regression line fitted to the data from the period before freezing. The blue dashed line in (b) is a regression line fitted to the data from the period after freezing.

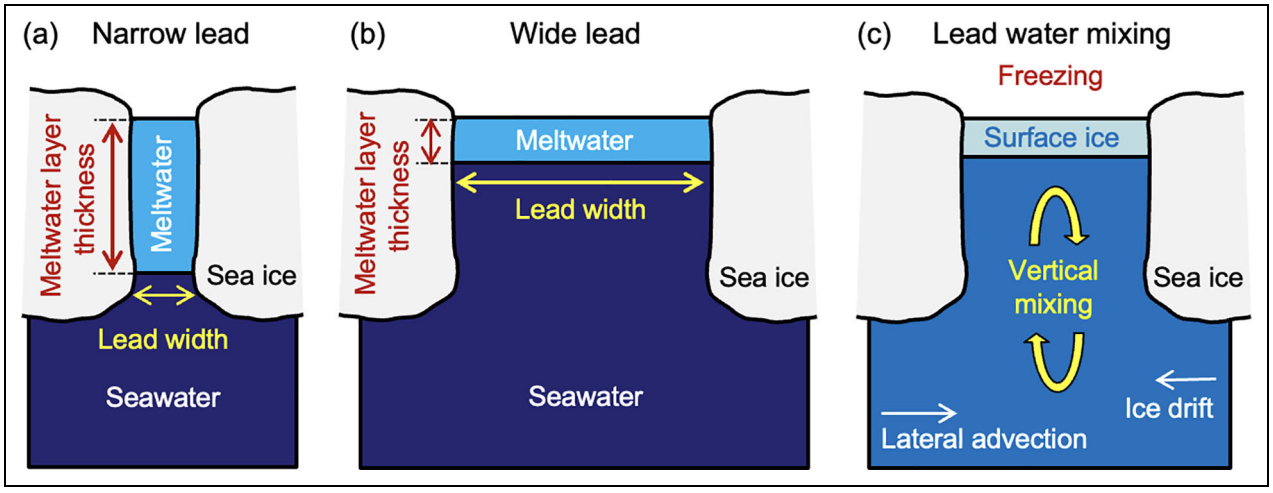

Figure 7. Schematic diagrams of the relationship between lead width and meltwater layer thickness. (a) When the lead is narrow, the meltwater layer is thick. (b) When the lead is wide, the meltwater layer is thin. (c) Schematic diagram of lead freezing and water mixing by lateral advection and ice drift.

changed significantly. On August 25, the lead began to narrow, and by September 1 it was only 5 m wide (**Figure 2d**), and during this period, the wind speed sometimes exceeded 10 m s^{-1}, with ice drift speed varying between 0 and 36 km d^{-1}. Furthermore, after September 1, although wind speed and ice drift speed showed different trends, lead width remained at 5 m. These results indicated that there was no clear relationship between changes in lead width, wind speed, or ice drift speed. However, ice dynamics for the port side lead of the R/V *Polarstern* (on the opposite side of the ship to our lead) changed dramatically during the study period: on September 13, the port side lead started to open up, widening to about 500 m on September 14 and closing again on September 15, and still some open water remained (Nicolaus et al., 2021). Therefore, although a relationship between changes in our lead width and changes in wind speed or ice drift speed was not clear, ice dynamics (e.g., its differential motion, diverging and converging) for the port side lead of the R/V *Polarstern* was related to the wind, especially during the second storm event (**Figure 2b**). A strong correlation ($r^2 = 0.60$, $p < 0.001$) between wind speed and ice drift speed supports this interpretation.

4.3. Lead freezing

As discussed in Section 4.2, the meltwater layer thickness prior to freezing could be explained by the change in lead width (**Figure 6a**). However, the decrease in meltwater layer thickness after freezing cannot be explained by lead width variation due to the fixed lead width of 5 m (**Figures 2d** and **6a**). Therefore, we examined ice formation in the lead after the onset of freezing due to the similarities

of this situation and that of the fifth stage described by Golovin and Ivanov (2015): steady ice formation in the lead and transition to winter conditions. Firstly, after freezing (September 1), the meltwater layer thickness decreased with the increasing thickness of ice on the lead surface (**Figure 2e** and **f**), resulting in a strong correlation ($r^2 = 0.82$, $p < 0.001$; **Figure 6b**). During ice formation, the higher freezing temperature of low-salinity meltwater would remove this layer from the surface water of the lead preferentially, decreasing the meltwater layer thickness. Meltwater layer thickness was approximately 0.42 m (the intercept of the regression line in **Figure 6b**) when freezing started. Therefore, if the disappearance of the meltwater layer after the onset of freezing was solely due to lead ice formation, the resulting ice thickness once stratification had broken down should have been 0.42 m (0.46 m if ice density was assumed to be 900 kg m^{-3} and volume increase during freezing was taken into account). However, maximum lead ice thickness was 0.2 m (**Figure 2f**). Therefore, only about 48% of the decrease in the meltwater layer thickness could be explained by ice formation in the lead (if volume increase during freezing was taken into account, 43% of the decrease in the meltwater layer thickness could be explained).

4.4. Water mixing

Water mixing within the lead is the most likely fate of the remaining meltwater. Therefore, we considered the effect of salinity on the density increase within the meltwater layer to examine density-driven water mixing within the lead. Ice in the lead was 0.2 m thick by the end of our survey period (**Figure 2d**). We hypothesize that the ice formation process produced an increase of below-ice salinity through the formation of brine channels in the ice and drainage of the brine from the ice into the underlying water. The salinity at depths of both 3 m and 10 m decreased by more than 2, from 31.6 on August 23 to 29.3 on September 17 (**Figure 5a**). We attributed this decrease to active vertical mixing of the meltwater layer at the surface with underlying water, which diluted the salinity at intermediate depths of the water column.

The following mass balance equation was used to calculate the salt budget within the surface mixed layer to a depth of 18.4 m (Kawaguchi et al., 2022) during Leg 5:

$$S_{\mathrm{fw}} V_{\mathrm{fw}} \rho_{\mathrm{fw}} + S_{\mathrm{sw\_bef.}} V_{\mathrm{sw\_bef.}} \rho_{\mathrm{sw\_bef.}} = S_{\mathrm{ice}} V_{\mathrm{ice}} \rho_{\mathrm{ice}} + S_{\mathrm{sw\_aft.}} V_{\mathrm{sw\_aft.}} \rho_{\mathrm{sw\_aft.}} \quad (4)$$

where S is salinity, V is volume per unit area, and ρ is density; the subscripts fw, sw, and ice refer to meltwater, seawater, and sea ice, respectively; and bef. and aft. indicate before freezing (e.g., August 23), and after freezing (e.g., September 17), respectively. We used the following observed data: $S_{\mathrm{fw}} = 2.6$, $V_{\mathrm{fw}} = 0.71$ m^3, $\rho_{\mathrm{fw}} = 1001.9$ kg m^{-3}, $S_{\mathrm{sw\_bef.}} = 32.2$, $V_{\mathrm{sw\_bef.}} = 17.7$ m^3, $\rho_{\mathrm{sw\_bef.}} = 1025.1$ kg m^{-3}, $V_{\mathrm{sw\_aft.}} = 18.2$ m^3, and $\rho_{\mathrm{sw\_aft.}} = 1023.6$ kg m^{-3} and treated $S_{\mathrm{sw\_aft.}}$ as an unknown. S_{ice} and V_{ice} were 4.3 and 0.2 m^3, respectively, at the end of the survey period (September 15 and 17); ρ_{ice} was assumed to be 900 kg m^{-3}. Using Equation 4, we calculated $S_{\mathrm{sw\_aft.}}$ to be 30.4, whereas the salinity measured at the end of the survey period (September 15) was 29.4 (**Figure 5a**). This result suggests that the salt budget within the surface mixed layer can explain only 64% of the decrease in the salinity by the dilution effect of the meltwater layer due to vertical mixing. Rather, the observed salinity balance infers that additional freshwater was added to the water column. Therefore, in the next section, we examine the possibility that a decrease in salinity was caused by the ice floe crossing a surface frontal structure that included a region with distinctly lower salinity from snowmelt water and river runoff.

4.5. Water mass variation under sea ice and disturbance of the lead water by wind-driven drifting of the ice floe

Figure 8 shows the temporal variation of the lead water on a T–S diagram. If mixing occurred only between meltwater at the surface of the lead and seawater, then the measured temperature and salinity of the mixed water should plot along a line connecting the seawater and meltwater values on the T–S diagram. However, most measured values during the second half of the survey period did not plot along the regression lines fitted to the data obtained during the first half of the survey period (**Figure 8b**). In addition, observed salinity and $\delta^{18}O$ values were lower during the second half of the survey period than during the first half (**Figure 5**). Furthermore, $\delta^{18}O$ of the surface water of the lead (−2.9‰) was higher than that of seawater after freezing (−3.2‰; **Figure 9a** and **b**). These results indicate that the mixing of lead meltwater with the underlying seawater cannot explain the lower $\delta^{18}O$ of seawater after freezing (−3.2‰). In addition, the intercept of a regression line fitted through the $\delta^{18}O$ versus salinity data of the seawater (**Figure 9b**) was −23.3‰ on the $\delta^{18}O$ axis (of **Figure 9a**). This $\delta^{18}O$ value is similar to that for the snow end-member (**Figure 9a**; **Table 2**) and for Arctic rivers (−20‰; Bauch et al., 1995). These results support our inference that the salt budget within the surface mixed layer cannot be explained alone by the dilution effect, and that additional freshwater (e.g., snow meltwater and river water) was added during the second half of the survey period.

Kawaguchi et al. (2022) reported that a decrease of seawater salinity was observed in the surface mixed layer at the end of August 2020 based on microstructure/turbulence measuring system (MSS) data from Schulz et al. (2022). They suggested that the abrupt freshening occurred when the ice floe moved across a surface frontal structure and entered a region where the surface mixed layer was dominated by fresh meltwater ($S < 29$). Their suggestion was that the lead water structure had been altered by this under-ice water, which had mixed with a different water mass as a result of the lateral advection and movement of the ice during Leg 5 (**Figure 7c**).

Golovin and Ivanov (2015) observed that the lower boundary of the pycnocline was disturbed during periods of intensive ice drift by turbulence in the under-ice drifting flow, which flows from the lower edge of the perennial ice into the lead as a free turbulent jet. The findings of this previous work suggest that sub-surface water masses affected the lead water properties observed in our study

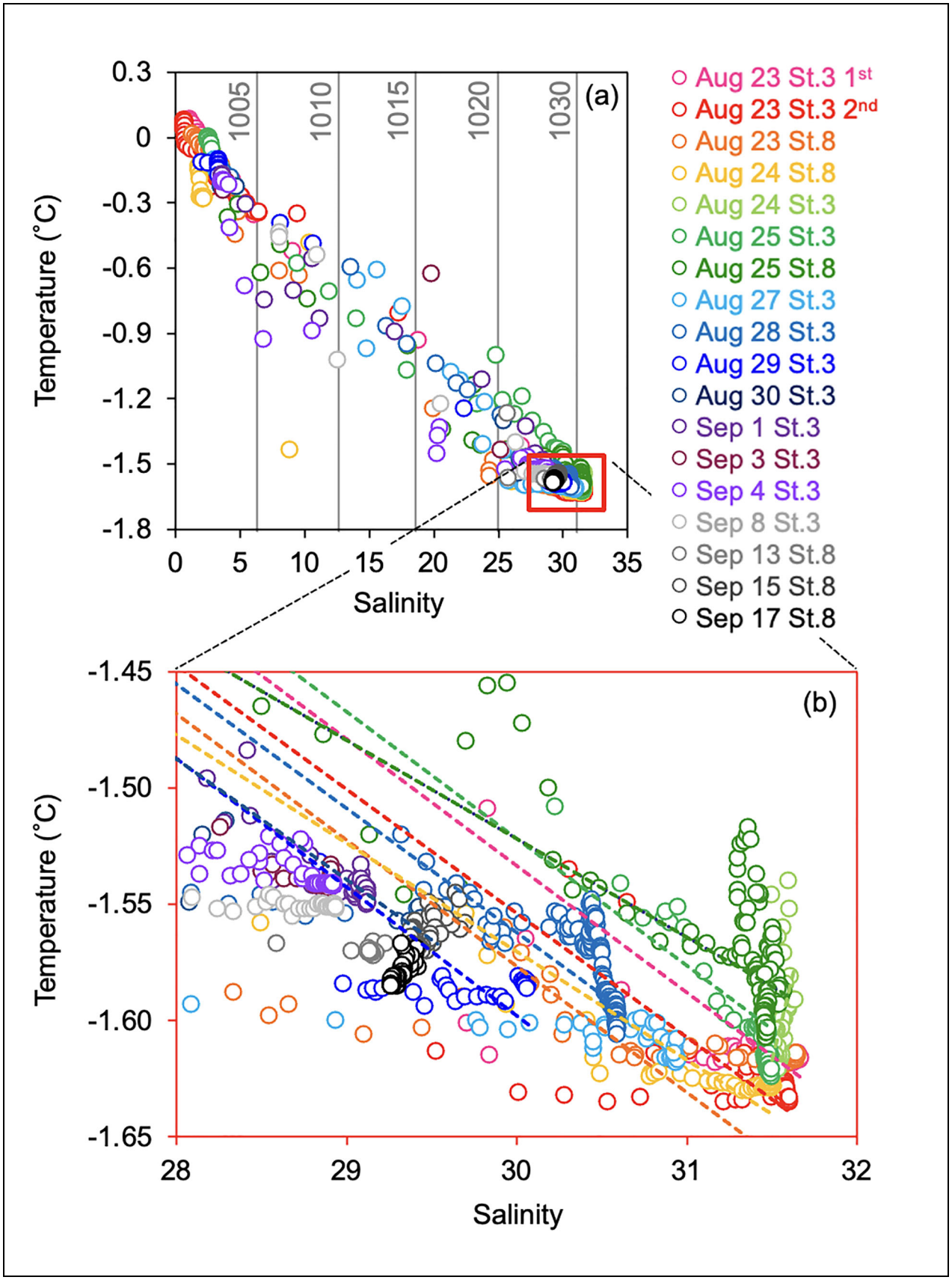

Figure 8. Temperature–salinity diagram of lead water. (a) Temperature–salinity (T–S) diagram of the lead water column and (b) enlarged view of a portion of the diagram in (a). Grey lines in (a) show the isopycnals at a given salinity. Dashed lines in (b) are regression lines fitted to the data from the period before freezing.

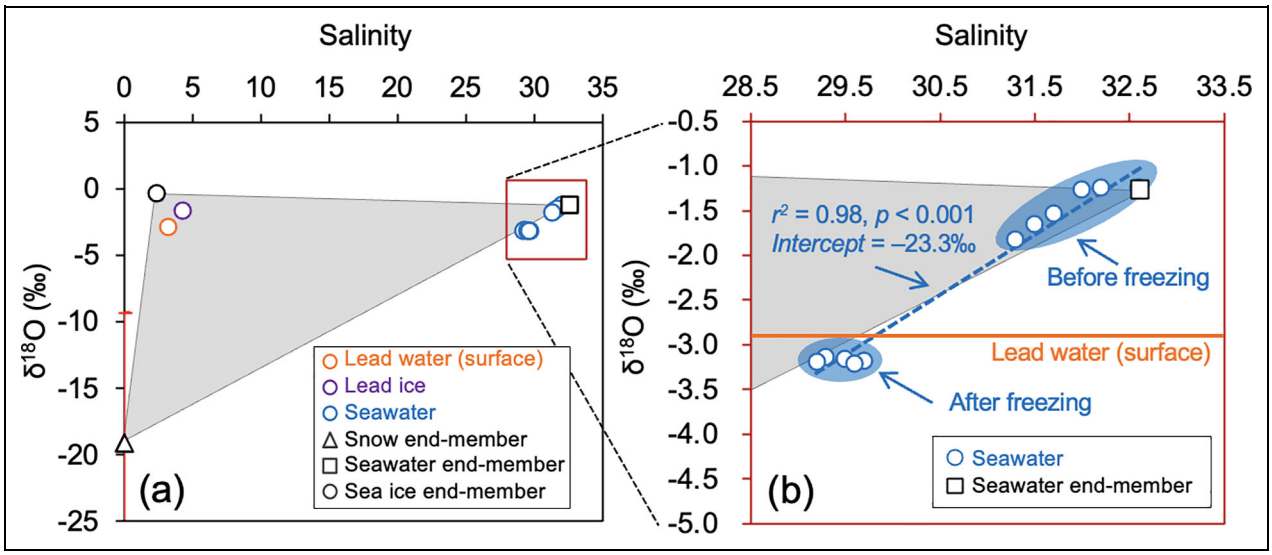

Figure 9. Relationship between $\delta^{18}O$ and salinity. (a) Relationship between $\delta^{18}O$ and salinity for surface lead water (August 29), lead ice (September 15), seawater (10 m depth), and end-members for snow, sea ice, and seawater (**Table 2**). (b) Enlarged view of a portion of the data in (a). Error bars (red) indicate standard deviation for each end-member; error bars are smaller size than the symbol size for sea ice and seawater end-members. The triangle shaded in grey shows the area enclosed by segments of the three end-members. The horizontal orange line in (b) indicates the $\delta^{18}O$ value of surface water in the lead. The blue dashed line in (b) is a regression line fitted to the data for seawater.

through turbulence driven by ice motion. In the second half of our survey period, high wind speeds exceeding 12 m s^{-1} were observed during the first storm (around September 7) and the second storm (around September 13 and 14; **Figure 2b**). Given the strong correlation (r^2 = 0.60, $p < 0.001$) between wind speed and ice drift speed, this interpretation is supported.

5. Summary and concluding remarks

To understand the effects of lead width, re-freezing, and mixing on the vertical structure of lead water during late summer in the central Arctic, we conducted a survey during the international drift campaign MOSAiC Leg 5. At the beginning of the survey period, the meltwater layer occupied the top 0.8 m of the lead waters, with strong stratification when the lead was narrow. However, as the survey period progressed, this strong stratification weakened, and the meltwater layer thickness was first reduced before it disappeared completely.

We found a strong negative correlation (r^2 = 0.77, $p <$ 0.001) between lead width and the meltwater layer thickness before freezing (**Figure 6a**). When the lead became narrow, the meltwater layer thickened, whereas when the lead expanded, the meltwater layer was stretched, and thinned (**Figure 7**) and then disappeared (**Figure 2d** and **e**; **Figure 3a** and **b**). On August 24, the salinity was approximately 31.6 throughout the upper water column. This result suggests that the meltwater layer was rapidly stretched by the lead width expansion that occurred prior to the measurement of the salinity profile on this day. At the same time, the water in the lead was vertically mixed by the sudden ice movement.

Ice formation reduced the meltwater layer thickness, as suggested by the strong negative correlation (r^2 = 0.82, $p <$ 0.001) between meltwater layer thickness and lead ice thickness (**Figure 6b**). The temperature–salinity diagram results (**Figure 8**) and the $\delta^{18}O$–salinity relationship in lead water (**Figure 9**) suggest that the water beneath the lead also affected lead water properties through turbulence driven by the motion of the ice floe.

Our findings suggest that the meltwater layer occupies the surface of the sea ice area in the Arctic Ocean, with profound implications for the season studied. During summer, this layer will modify the ocean–atmosphere fluxes for heat, gases, and particles, such as sea salt. In addition, snow and sea ice meltwater, as well as precipitation and river runoff (Carmack et al., 2015), result in lower salinity and stratification of the upper layer of the Arctic Ocean. In general, this stratification regulates and constrains physical and biogeochemical processes and atmospheric exchange, which will be affected by the dynamic nature of the meltwater layer. Therefore, our exploration of the meltwater dynamics in a lead should improve our understanding of the future Arctic Ocean, which is expected to be characterized by increased meltwater inputs (McPhee et al., 2009; Rabe et al., 2011).

Data accessibility statement

The data analyzed in this study were mainly retrieved from links below: RINKO profiler-derived variables: https://doi.pangaea.de/10.1594/PANGAEA.945337, water sampling derived variables: https://doi.pangaea.de/10.1594/PANGAEA.945285, meteorological variables: https://doi.org/10.1594/PANGAEA.935267, and MSS profiler-derived variables: https://doi.org/10.1594/PANGAEA.939816. The oxygen isotope data stems from the ISOLAB Facility at AWI in Potsdam.

Acknowledgments

This work was conducted and data used for this report were produced as part of the international Multidisciplinary drifting Observatory for the Study of the Arctic Climate (MOSAiC) with the tag MOSAiC20192020. We thank all persons involved in the expedition of the R/V *Polarstern* during MOSAiC in 2019–2020 (AWI_PS122_00) as listed in Nixdorf et al. (2021; http://doi.org/10.5281/zenodo.5179739) and Manami Tozawa for making the map for **Figure 1b**.

Funding

This study was supported by the Japan Society for the Promotion of Science (grant numbers: JP18H03745; JP18KK0292; JP17KK0083; JP17H04715; JP20H04345) and by a grant from the Joint Research Program of the Japan Arctic Research NetworkCenter. MM and HM are supported through the German Federal Ministry of Education and Research (grant number 03FO869A). ALW and KS were funded through the UK Natural Environment Research Council (NERC) (Grants No NE/S002596/1 and NE/S002502/1, respectively). ESD was supported by NERC through the EnvEast Doctoral Training Partnership (NE/L002582/1), as well as NERC and the Department for Business, Energy & Industrial Strategy (BEIS) through the UK Arctic Office. EJC was supported by the National Science Foundation (USA) NSF OPP 1821911 and NSF Graduate Research Fellowship. CG was funded through the Spanish funding Agency (AEI) though the grant PCI 2019-111844-2. MMS was funded through NSF OPP-1724467, OPP-1724748, and OPP-2138787. DB was funded through the German funding Agency (DFG) through grant BA1689/4-1.

Competing interests

The authors declare that they have no conflict of interest.

Author contributions

Contributed to conception and design: DN, YK, ALW, ESD, EJC, BD.

Contributed to acquisition of data: DN, ALW, YL, MD, KS, ESD, EJC, NK, ES, MH, MRG.

Contributed to analysis and interpretation of data: DN, YK, HM, MM, DB.

Drafted and/or revised the article: DN drafted the first version of the manuscript, and all authors contributed to writing and revisions.

Approved the submitted version for publication: All authors.

References

Assmy, P, **Fernandez-Mendez, M**, **Duarte, P**, **Meyer, A**, **Randelhoff, A**, **Mundy, CJ**, **Olsen, LM**, **Kauko, HM**, **Bailey, A**, **Chierici, M**, **Cohen, L**, **Doulgeris, AP**, **Ehn, JK**, **Fransson, A**, **Gerland, S**, **Hop, H**, **Hudson, SR**, **Hughes, N**, **Itkin, P**, **Johnsen, G**, **King, JA**, **Koch, BP**, **Koenig, Z**, **Kwasniewski, S**, **Laney, SR**, **Nicolaus, M**, **Pavlov, AK**, **Polashenski, CM**, **Provost, C**, **Rosel, A**, **Sandbu, M**, **Spreen, G**, **Smedsrud, LH**, **Sundfjord, A**, **Taskjelle, T**, **Tatarek, A**, **Wiktor, J**, **Wagner, PM**, **Wold, A**, **Steen, H**, **Granskog, MA.** 2017. Leads in Arctic pack ice enable early phytoplankton blooms below snow covered sea ice. *Scientific Reports* **7**. DOI: http://doi.org/10.1038/srep40850.

Baccarini, A, **Karlsson, L**, **Dommen, J**, **Duplessis, P**, **Vüllers, J**, **Brooks, IM**, **Saiz-Lopez, A**, **Salter, M**, **Tjernström, M**, **Baltensperger, U**, **Zieger, P**, **Schmale, J**. 2020. Frequent new particle formation over the high Arctic pack ice by enhanced iodine emissions. *Nature Communications* **11**: 4924. DOI: https://doi.org/10.1038/s41467-020-18551-0.

Bauch, D, **Schlosser, P**, **Fairbanks, RF.** 1995. Freshwater balance and the sources of deep and bottom waters in the Arctic Ocean inferred from the distribution of $H_2{}^{18}O$. *Progress in Oceanography* **35**: 53–80. DOI: http://doi.org/10.1016/0079-6611(95)00005-2.

Beck, L, **Sarnela, N**, **Junninen, H**, **Hoppe, CJM**, **Garmash, O**, **Bianchi, F**, **Riva, M**, **Rose, C**, **Peräkylä, O**, **Wimmer, D**, **Kausiala, O**, **Jokinen, T**, **Ahonen, L**, **Mikkilä, J**, **Hakala, L**, **He, HU**, **Kontkanen, J**, **Wolf, KKE**, **Cappelletti, D**, **Sipilä, M**. 2021. Differing mechanisms of new particle formation at two Arctic sites. *Geophysical Research Letters* **48**(4): e2020GL091334. DOI: https://doi.org/10.1029/2020GL091334.

Carmack, EC, **Yamamoto-Kawai, M**, **Haine, TWN**, **Bacon, S**, **Bluhm, BA**, **Lique, C**, **Melling, H**, **Polyakov, IV**, **Straneo, F**, **Timmermans, M-L**, **Williams, WJ**. 2016. Freshwater and its role in the Arctic Marine System: Sources, disposition, storage, export, and physical and biogeochemical consequences in the Arctic and global oceans. *Journal of Geophysical Research: Biogeosciences* **121**: 675–717. DOI: https://doi.org/10.1002/2015JG003140.

Eicken, H. 1994. Structure of under-ice melt ponds in the central Arctic and their effect on the sea-ice cover. *Limnology and Oceanography* **39**: 682–694. DOI: https://doi.org/10.4319/lo.1994.39.3.0682.

Eicken, H, **Krouse, HR**, **Kadko, D**, **Perovich, DK**. 2002. Tracer studies of pathways and rates of meltwater transport through Arctic summer sea ice. *Journal of Geophysical Research: Oceans* **107**(C10): SHE–22. DOI: http://doi.org/10.1029/2000JC000583.

Fransson, A, **Chierici, M**, **Skjelvan, I**, **Olsen, A**, **Assmy, P**, **Peterson, AK**, **Ward, B.** 2017. Effects of sea-ice and biogeochemical processes and storms on under-ice water fCO_2 during the winter-spring transition in the high Arctic Ocean: Implications for sea–air CO_2 fluxes. *Journal of Geophysical Research: Oceans* **122**: 5566–5587. DOI: https://doi.org/10.1002/2016JC012478.

Golovin, PN, **Ivanov, VV**. 2015. Density stratification effects on the ice lead heat balance and perennial ice melting in the Central Arctic. *Russian Meteorology and Hydrology* **40**(1): 46–59. DOI: http://doi.org/10.3103/S1068373915010070.

Inoue, J, **Kikuchi T.** 2006. Effect of summertime wind conditions on lateral and bottom melting in the

central Arctic. *Annals of Glaciology* **44**: 37–41. DOI: http://doi.org/10.3189/172756406781811231.

Itkin, P, **Spreen, G**, **Cheng, B**, **Doble, M**, **Girard-Ardhuin, F**, **Haapala, J**, **Hughes, N**, **Kaleschke, L**, **Nicolaus, M**, **Wilkinson, J**. 2017. Thin ice and storms: Sea ice deformation from buoy arrays deployed during N-ICE2015. *Journal of Geophysical Research: Oceans* **122**: 4661–4674. DOI: http://doi.org/10.1002/2016JC012403.

Kauko, HM, **Taskjelle, T**, **Assmy, P**, **Pavlov, AK**, **Mundy, CJ**, **Duarte, P**, **Fernández-Méndez, M**, **Olsen, LM**, **Hudson, SR**, **Johnsen, G**, **Elliott, A**, **Wang Granskog, MA**. 2017. Windows in Arctic sea ice: Light transmission and ice algae in a refrozen lead. *Journal of Geophysical Research: Biogeosciences* **122**(6): 1486–1505. DOI: http://doi.org/10.1002/2016JG003626.

Kawaguchi, Y, **Koenig, Z**, **Nomura, D**, **Hoppman, M**, **Inoue, J**, **Fang, Y-C**, **Schulz, K**, **Katlein, C**, **Nicolaus, M**, **Rabe, B**. 2022. Turbulent mixing during late summer in the ice–ocean boundary layer in the central Arctic Ocean: Results from the MOSAiC expedition. *Journal of Geophysical Research: Oceans* **127**(8): e2021JC017975. DOI: https://doi.org/10.1029/2021JC017975.

Kwok, R. 2018. Arctic sea ice thickness, volume, and multiyear ice coverage: Losses and coupled variability (1958–2018). *Environmental Research Letters* **13**: 105005. DOI: http://doi.org/10.1088/1748-9326/aae3ec.

Lange, BA, **Salganik, E**, **Macfarlane, A**, **Schneebeli, M**, **Høyland, K**, **Gardner, J**, **Müller, O**, **Divine, DV**, **Kohlbach, D**, **Katlein, C**, **Granskog, M**. n.d. Snowmelt contributes to first-year ice ridge consolidation during summer melt. *Elementa: Science of the Anthropocene*, submitted, under review.

Lindsay, R, **Schweiger, A.** 2015. Arctic sea ice thickness loss determined using subsurface, aircraft, and satellite observations. *The Cryosphere* **9**(1): 269–283. DOI: http://doi.org/10.5194/tc-9-269-2015.

Loose, B, **McGillis, WR**, **Perovich, D**, **Zappa, CZ**, **Schlosser, P.** 2014. A parameter model of gas exchange for the seasonal sea ice zone. *Ocean Science* **10**(1): 17–28. DOI: https://doi.org/10.5194/os-10-17-2014.

Maykut, GA. 1978. Energy exchange over young sea ice in the central Arctic. *Journal of Geophysical Research* **83**(C7): 3646–3658. DOI: https://doi.org/10.1029/JC083iC07p03646.

McPhee, MG, **Proshutinsky, A**, **Morison, JH**, **Steele, M**, **Alkire, MB**. 2009. Rapid change in freshwater content of the Arctic Ocean. *Geophysical Research Letters* **36**: L10602. DOI: https://doi.org/10.1029/2009GL037525.

Meier, WN, **Hovelsrud, GK**, **van Oort, BEH**, **Key, JR**, **Kovacs, KM**, **Michel, C**, **Haas, C**, **Granskog, MA**, **Gerland, S**, **Perovich, DK**, **Makshtas, A**, **Reist, JD**. 2014. Arctic sea ice in transformation: A review of recent observed changes and impacts on biology and human activity. *Review of Geophysics* **52**: 185–217. DOI: http://doi.org/10.1002/2013RG000431.

Meyer, H, **Mellat, M**, **Nomura, D**, **Damm, E**, **Bauch, D**, **Weiner, M**, **Marent, A.** 2022. Stable water isotopes and conductivities of a lead case study during Leg 5 of the MOSAiC expedition. PANGAEA. DOI: https://doi.org/10.1594/PANGAEA.945285.

Meyer, H, **Schönicke, L**, **Wand, U**, **Hubberten, H-W**, **Friedrichsen, H**. 2000. Isotope studies of hydrogen and oxygen in ground ice—Experiences with the equilibration technique. *Isotopes in Environmental and Health Studies* **36**(2): 133–149. DOI: https://doi.org/10.1080/10256010008032939.

Morison, JH, **McPhee, MG**. 1998. Lead convection measured with an autonomous underwater vehicle. *Journal Geophysical Research: Oceans* **103**: 3257–3281. DOI: https://doi.org/10.1029/97JC02264.

Morison, JH, **McPhee, MG**, **Curtin, TB**, **Paulson, CA.** 1992. The oceanography of winter leads. *Journal Geophysical Research: Oceans* **97**: 11199–11218. DOI: https://doi.org/10.1029/92JC00684.

Nansen, F. 1902. The oceanography of the North Polar Basin, The Norwegian North Polar Expedition 1893–1896. *Scientific Results* **3**: 1–427.

Nicolaus, M, **Arndt, S**, **Birnbaum, G**, **Katlein, C**. 2021. Visual panoramic photographs of the surface conditions during the MOSAiC campaign 2019/20. PANGAEA. DOI: https://doi.org/10.1594/PANGAEA.938534.

Nicolaus, M, **Perovich, DK**, **Spreen, G**, **Granskog, MA**, **von Albedyll, L**, **Anhaus, P**, **Angelopoulos, M**, **Arndt, A**, **Belter, HJ**, **Bessonov, V**, **Birnbaum, G**, **Brauchle, JB**, **Calmer, R**, **Cardellach, E**, **Cheng, B**, **Clemens-Sewall, D**, **Dadic, R**, **Damm, E**, **de Boer, G**, **Demir, O**, **Divine, D**, **Fong, A**, **Fons, S**, **Fuchs, N**, **Gabarro, C**, **Gerland, S**, **Gradinger, R**, **Goessling, HF**, **Haapala, J**, **Haas, C**, **Hamilton, J**, **Hannula, HR**, **Hendricks, S**, **Herber, A**, **Heuze, C**, **Hoppmann, M**, **Hyland, KV**, **Huntemann, M**, **Hutchings, JK**, **Hwang, B**, **Itkin, P**, **Jaggi, M**, **Jutila, A**, **Kaleschke, L**, **Katlein, C**, **Kolabutin, N**, **Krampe, D**, **Kristensen, SS**, **Krumpen, T**, **Kurtz, N**, **Lampert, A**, **Lange, BA**, **Lei, R**, **Light, B**, **Linhardt, F**, **Liston, G**, **Loose, B**, **Macfarlane, AR**, **Mahmud, M**, **Matero, IO**, **Maus, S**, **Morgenstern, A**, **Naderpour, R**, **Nandan, V**, **Niubom, A**, **Oggier, M**, **Oppelt, N**, **Patzold, F**, **Petrovsky, T**, **Pirazzini, R**, **Polashenski, C**, **Rabe, B**, **Raphael, IA**, **Regnery, J**, **Rex, M**, **Ricker, R**, **Riemann-Campe, K**, **Rinke, A**, **Rohde, J**, **Salganik, E**, **Scharien, RK**, **Schiller, M**, **Schneebeli, M**, **Semmling, M**, **Sheikin, I**, **Shimanchuk, E**, **Shupe, MD**, **Smith, MM**, **Smolyanitsky, V**, **Sokolov, V**, **Sokolova, J**, **Stanton, TP**, **Stroeve, J**, **Tavri, A**, **Thielke, L**, **Timofeeva, A**, **Tonboe, RT**, **Tsamados, M**, **Wagner, DN**, **Watkins, D**, **Webster, M**, **Wendisch, M**. 2022. Overview of the MOSAiC expedition: Snow and sea ice. *Elementa: Science of the Anthropocene* **10**(1). DOI: https://doi.org/10.1525/elementa.2021.000046.

Nixdorf, U, **Dethloff, K**, **Rex, M**, **Shupe, M**, **Sommerfeld, A**, **Perovich, D**, **Nicolaus, M**, **Heuze, C**, **Rabe, B**, **Loose, B**, **Damm, E**, **Gradinger, R**, **Fong, A**, **Maslowski, W**, **Rinke, A**, **Kwok, R**, **Spreen, G**, **Wendisch, M**, **Herber, A**, **Hirsekorn, M**, **Mohaupt, V**, **Frickenhaus, S**, **Immerz, A**, **Weiss-Tuider, K**, **Konig, B**, **Mengedoht, D**, **Regnery, J**, **Gerchow, P**, **Ransby, D**, **Krumpen, T**, **Morgenstern, A**, **Haas, C**, **Kanzow, T**, **Rack, FR**, **Saitzev, V**, **Sokolov, V**, **Makarov, A**, **Schwarze, S**, **Wunderlich, T**, **Wurr, K**, **Boetius, A**. 2021. MOSAiC extended acknowledgement. Zenodo. DOI: http://doi.org/10.5281/zenodo.5179739.

Nomura, D, **Aoki, S**, **Simizu, D**, **Iida, T**. 2018. Influence of sea ice crack formation on the spacial distribution of nutrients and microalgae in flooded Antarctic multiyear ice. *Journal of Geophysical Research: Oceans* **123**(2): 939–951. DOI: http://doi.org/10.1002/2017JC012941.

Nomura, D, **Kawaguchi, Y**, **Hoppmann, M**, **Damm, E**, **Li, Y**. 2022. Profiles of temperature, salinity and dissolved oxygen measured by a handheld CTD in a lead during MOSAiC Leg PS122/5 to the central Arctic in August-September 2020. PANGAEA. DOI: https://doi.org/10.1594/PANGAEA.945337.

Nomura, D, **Takatsuka, T**, **Ishikawa, M**, **Kawamura, T**, **Shirasawa, K**, **Yoshikawa-Inoue, H**. 2009. Transport of chemical components in sea ice and under-ice water during melting in the seasonally ice-covered Saroma-ko Lagoon, Hokkaido, Japan. *Estuarine, Coastal and Shelf Science* **81**: 201–209. DOI: https://doi.org/10.1016/j.ecss.2008.10.012.

Ólason, E, **Rampal, P**, **Dansereau, V**. 2021. On the statistical properties of sea-ice lead fraction and heat fluxes in the Arctic. *The Cryosphere* **15**: 1053–1064. DOI: https://doi.org/10.5194/tc-15-1053-2021.

Østlund, HG, **Hut, G**. 1984. Arctic Ocean water mass balance from isotope data. *Journal of Geophysical Research* **89**(C4): 6373–6381. DOI: http://doi.org/10.1029/JC089iC04p06373.

Parmentier, FJW, **Christensen, TR**, **Srensen, LL**, **Rysgaard, S**, **McGuire, AD**, **Miller, PA**, **Walker, DA**. 2013. The impact of lower sea-ice extent on Arctic greenhouse-gas exchange. *Nature Climate Change* **3**: 195–202. DOI: http://doi.org/10.1038/nclimate1784.

Perovich, DK, **Maykut, GA**. 1990. Solar heating of a stratified ocean in the presence of an ice cover. *Journal of Geophysical Research* **95**: 18233–18245. DOI: https://doi.org/10.1029/JC095iC10p18233.

Petrich, C, **Langhorne, PJ**, **Haskell, TG**. 2007. Formation and structure of refrozen cracks in land-fast first-year sea ice. *Journal of Geophysical Research* **112**: C04006. DOI: http://doi.org/10.1029/2006JC003466.

Rabe, B, **Heuze, C**, **Regnery, J**, **Aksenov, Y**, **Allerholt, J**, **Athanase, M**, **Bai, Y**, **Basque, C**, **Bauch, D**, **Baumann, TM**, **Chen, D**, **Cole, ST**, **Craw, L**, **Davies, A**, **Damm, E**, **Dethloff, K**, **Divine, DV**, **Doglioni, F**, **Ebert, F**, **Fang, Y-C**, **Fer, I**, **Fong, AA**, **Gradinger, R**, **Granskog, MA**, **Groupner, R**, **Haas, C**, **He, H**, **He, Y**, **Hoppmann, M**, **Janout, M**, **Kadko, D**, **Kanzow, T**, **Karam, S**, **Kawaguchi, Y**, **Koenig, Z**, **Kong, B**, **Krishfield, RA**, **Kuhlmey, D**, **Kuznetsov, I**, **Lan, M**, **Lei, R**, **Li, T**, **Torres-Valdes, S**, **Lin, L**, **Lin, L**, **Liu, H**, **Liu, N**, **Loose, B**, **Ma, X**, **MacKay, R**, **Mallet, M**, **Mallett, RDC**, **Maslowski, W**, **Mertens, C**, **Mohrholz, V**, **Muilwijk, M**, **Nicolaus, M**, **O'Brien, JK**, **Perovich, D**, **Ren, J**, **Rex, M**, **Ribeiro, N**, **Rinke, A**, **Schaffer, J**, **Schuffenhauer, I**, **Schulz, K**, **Shupe, MD**, **Shaw, W**, **Sommerfeld, A**, **Spreen, G**, **Stanton, T**, **Stephens, M**, **Su, J**, **Sukhikh, N**, **Sundfjord, A**, **Tippenhauer, S**, **Toole, JM**, **Vredenborg, M**, **Walter, M**, **Wang, H**, **Wang, L**, **Wang, Y**, **Wendisch, M**, **Zhao, J**, **Zhou, M**, **Zhu, J**. 2022. Overview of the MOSAiC expedition: Physical oceanography. *Elementa: Science of the Anthropocene* **10**(1). DOI: https://doi.org/10.1525/elementa.2021.00062.

Rabe, B, **Karcher, M**, **Schauer, U**, **Toole, JM**, **Krishfield, RA**, **Pisarev, S**, **Kauker, F**, **Gerdes, R**, **Kikuchi, T**. 2011. An assessment of Arctic Ocean meltwater content changes from the 1990s to the 2006–2008 period. *Deep Sea Research Part I: Oceanographic Research Papers* **58**(2): 173–185. DOI: http://doi.org/10.1016/j.dsr.2010.12.002.

Rampal, P, **Weiss, J**, **Dubois, C**, **Campin, J-M**. 2011. IPCC climate models do not capture Arctic sea ice drift acceleration: Consequences in terms of projected sea ice thinning and decline. *Journal of Geophysical Research: Oceans* **116**: C00D07. DOI: http://doi.org/10.1029/2011JC007110.

Rex, M. 2021. Master tracks in different resolutions of POLARSTERN cruise PS122/5, Arctic Ocean - Bremerhaven, 2020-08-12 - 2020-10-12. Alfred Wegener Institute, Helmholtz Centre for Polar and Marine Research, Bremerhaven, PANGAEA. DOI: https://doi.org/10.1594/PANGAEA.926910.

Richter-Menge, JA, **Perovich, DK**, **Pegau, WS**. 2001. Summer ice dynamics during SHEBA and its effect on the ocean heat content. *Annals of Glaciology* **33**: 201–206. DOI: https://doi.org/10.3189/172756401781818176.

Schmithüsen, H, **Raeke, A**, **Wenzel, J**. 2021. Meteorological observations during POLARSTERN cruise PS122/5. Alfred Wegener Institute, Helmholtz Centre for Polar and Marine Research, Bremerhaven, PANGAEA. DOI: https://doi.org/10.1594/PANGAEA.935267.

Schulz, K, **Mohrholtz, V**, **Fer, I**, **Janout, M**, **Hoppman, M**, **Schaffer, J**, **Koenig, Z**. 2022. A full year of turbulence measurements from a drift campaign in the Arctic Ocean 2019–2020. *Scientific Data* **9**: 472. DOI: https://doi.org/10.1038/s41597-022-01574-1.

Shupe, MD, **Rex, M**, **Blomquist, B**, **Persson, POG**, **Schmale, J**, **Uttal, T**, **Althausen, D**, **Angot, H**, **Archer, S**, **Bariteau, L**, **Beck, I**, **Bilberry, J**, **Bucci, S**, **Buck, C**, **Boyer, M**, **Brasseur, Z**, **Brooks, IM**, **Calmer, R**, **Cassano, J**, **Castro, V**, **Chu, D**, **Costa, D**, **Cox, CJ**, **Creamean, J**, **Crewell, S**, **Dahlke, S**, **Damm, E**, **de Boer, G**, **Deckelmann, H**, **Dethloff, K**, **Dutsch, M**, **Ebell, K**, **Ehrlich, A**, **Ellis, J**,

Engelmann, R, **Fong, AA**, **Frey, MM**, **Gallagher, MR**, **Ganzeveld, L**, **Gradinger, R**, **Graeser, J**, **Greenamyer, V**, **Griesche, H**, **Griffiths, S**, **Hamilton, J**, **Heinemann, G**, **Helmig, D**, **Herber, A**, **Heuze, C**, **Hofer, J**, **Houchens, T**, **Howard, D**, **Inoue, J**, **Jacobi, H-W**, **Jaiser, R**, **Jokinen, T**, **Jourdan, O**, **Jozef, G**, **King, W**, **Kirchgaessner, A**, **Klingebiel, M**, **Krassovski, M**, **Krumpen, T**, **Lampert, A**, **Landing, W**, **Laurila, T**, **Lawrence, D**, **Lonardi, M**, **Loose, B**, **Lupkes, C**, **Maahn, M**, **Macke, A**, **Maslowski, W**, **Marsay, C**, **Maturilli, M**, **Mech, M**, **Morris, S**, **Moser, M**, **Nicolaus, M**, **Ortega, P**, **Osborn, J**, **Patzold, F**, **Perovich, DK**, **Petaja, T**, **Pilz, C**, **Pirazzini, R**, **Posman, K**, **Powers, H**, **Pratt, KA**, **Preuer, A**, **Quelever, L**, **Radenz, M**, **Rabe, B**, **Rinke, A**, **Sachs, T**, **Schulz, A**, **Siebert, H**, **Silva, T**, **Solomon, A**, **Sommerfeld, A**, **Spreen, G**, **Stephens, M**, **Stohl, A**, **Svensson, G**, **Uin, J**, **Viegas, J**, **Voigt, C**, **von der Gathen, P**, **Wehner, B**, **Welker, JM**, **Wendisch, M**, **Werner, M**, **Xie, ZQ**, **Yue, F.** 2022. Overview of the MOSAiC expedition: Atmosphere. *Elementa: Science of the Anthropocene* **10**(1). DOI: http://doi.org/10.1525/elementa.2021.00060.

Silyakova, A, **Nomura, D**, **Kotovitch, M**, **Fransson, A**, **Delille, B**, **Chierici, M**, **Granskog, MA**. 2022. Methane release from open leads and new ice following an Arctic winter storm event. *Polar Science* **33**: 100874. DOI: https://doi.org/10.1016/j.polar.2022.100874.

Smith, MM, **von Albedyll, L**, **Raphael, IA**, **Lange, BA**, **Matero, I**, **Salganik, E**, **Webster, MA**, **Granskog, MA**, **Fong, A**, **Lei, R**, **Light, B**. 2022. Quantifying false bottoms and under-ice meltwater layers beneath Arctic summer sea ice with fine-scale observations. *Elementa: Science of the Anthropocene* **10**(1). DOI: https://doi.org/10.1525/elementa.2021.000116.

Spreen, G, **Kwok, R**, **Menemenlis, D**. 2011. Trends in Arctic sea ice drift and role of wind forcing: 1992–2009. *Geophysical Research Letters* **38**: L19501. DOI: http://doi.org/10.1029/2011GL048970.

Steiner, NS, **Lee, WG**, **Christian, JR**. 2013. Enhanced gas fluxes in small sea ice leads and cracks: Effects on CO_2 exchange and ocean acidification. *Journal of Geophysical Research: Oceans* **118**: 1195–1205. DOI: http://doi.org/10.1002/jgrc.20100.

Stroeve, JC, **Serreze, MC**, **Holland, MM**, **Kay, JE**, **Maslanik, J**, **Barrett, AP**. 2012. The Arctic's rapidly shrinking sea ice cover: A research synthesis. *Climatic Change* **110**: 1005. DOI: http://doi.org/10.1007/s10584-011-0101-1.

Wilchinsky, AV, **Heorton, HDBS**, **Feltham, D**, **Holland, PR**. 2015. Study of the impact of ice formation in leads upon the sea ice pack mass balance using a new frazil and grease ice parameterization. *Journal of Physical Oceanography* **45**(8): 2025–2047. DOI: https://doi.org/10.1175/JPO-D-14-0184.1.

Willis, MD, **Leaitch, WR**, **Abbatt, JPD**. 2018. Processes controlling the composition and abundance of Arctic aerosol. *Review of Geophysics* **56**: 621–671. DOI: https://doi.org/10.1029/2018RG000602.

Zemmelink, HJ, **Houghton, L**, **Dacey, JWH**, **Worby, AP**, **Liss, PS**. 2005. Emission of dimethylsulfide from Weddell Sea leads. *Geophysical Research Letters* **32**: L23610. DOI: http://doi.org/10.1029/2005GL024242.

How to cite this article: Nomura, D, Kawaguchi, Y, Webb, AL, Li, Y, Dall'osto, M, Schmidt, K, Droste, ES, Chamberlain, EJ, Kolabutin, N, Shimanchuk, E, Hoppmann, M, Gallagher, MR, Meyer, H, Mellat, M, Bauch, D, Gabarró, C, Smith, MM, Inoue, J, Damm, E, Delille, B. 2023. Meltwater layer dynamics in a central Arctic lead: Effects of lead width, re-freezing, and mixing during late summer. *Elementa: Science of the Anthropocene* 11(1). DOI: https://doi.org/10.1525/elementa.2022.00102

Domain Editor-in-Chief: Jody W. Deming, University of Washington, Seattle, WA, USA

Guest Editor: Gunnar Spreen, Institute of Environmental Physics, University of Bremen, Bremen, Germany

Knowledge Domain: Ocean Science

Part of an Elementa Special Feature: The Multidisciplinary Drifting Observatory for the Study of Arctic Climate (MOSAiC)

Published: May 15, 2023 **Accepted:** March 24, 2023 **Submitted:** August 04, 2022